Research Square

Preprints are preliminary reports that have not undergone peer review.
They should not be considered conclusive, used to inform clinical practice,
or referenced by the media as validated information.

DFT study of the possible mechanisms for the synthesis of α-cyanophosphonates from β- nitrostyrenes

Hossein Tavakol (h_tavakol@iut.ac.ir)
Isfahan University of Technology
Sima shamsaddinimotlagh
Isfahan University of Technology
Arash Kazemi
Isfahan University of Technology

Research Article

Keywords: Mechanism, DFT, α-cyano phosphonate, triphenyl phosphite, β-nitrostyrene.

Posted Date: December 13th, 2023

DOI: https://doi.org/10.21203/rs.3.rs-3737180/v1

License: This work is licensed under a Creative Commons Attribution 4.0 International License. Read Full License

Additional Declarations: No competing interests reported.

Abstract

In this article, the theoretical study of the reaction mechanism of the addition of triphenyl phosphite to β-nitrostyrene is discussed. The M062X method, which is a subset of density functional theory (DFT) and def2svp basis set, was used to determine the appropriate mechanism. To accomplish this, the structures of the starting materials, products, intermediates, and transition states were optimized, and their respective energies were obtained. For this purpose, three plausible reaction mechanisms were proposed, denoted as paths a, b, and c. In the pathway a, triphenyl phosphite is added to the β-position of β-nitrostyrene. The b pathway is designed in such that the triphenyl phosphite molecule is added to the oxygen of nitro in β-nitrostyrene, and in the c pathway, triphenyl phosphite is added to the nitrogen of the β-nitrostyrene compound. Since the presence of two ml mol of triphenyl phosphite is required to carry out the reaction and form the desired product, all three routes of the proposed mechanism were designed accordingly. by evaluating potential reaction pathways and comparing their energetics, a plausible mechanism for the reaction can be proposed.

1. Introduction

For chemists, comprehending the intricate mechanisms of organic reactions has been a significant subject for a considerable period of time. to acquire a thorough comprehension of reaction mechanisms, chemists have utilized a diverse array of experimental techniques that incorporate spectroscopic, analytical and physical instruments. these methods have played a crucial role in furnishing ample details necessary for elucidating the mechanisms of various reactions. indeed, the experimental investigation of reaction mechanisms can be time-consuming and demanding in terms of laboratory equipment and costs. the need for extensive resources and the associated expenses can pose challenges to conducting thorough experimental studies. this is where computational methods can offer a cost-effective and efficient alternative, allowing for the exploration of reaction mechanisms without the same level of resource requirements. as a result, the experimental investigation of the mechanism behind certain chemical reactions can be challenging or, in some cases, even impossible [1–6]. In recent years, computational or theoretical methods have undergone significant advancements and have been extensively utilized for studying diverse chemical systems, investigating reaction mechanisms, and predicting their behaviors. theses computational approaches have proven to be valuable tools in complementing experimental studies and providing insights into complex chemical processes. Indeed, these computational methods have proven to be valuable in predicting reaction mechanisms and providing substantial evidence to support them [7–9]. they can be used independently or in conjunction with experimental methods to enhance our understanding of chemical reactions. By utilizing computational techniques, scientists can make predictions, simulate reactions, and validate their findings, thereby contributing to the advancement of our knowledge in the field of chemistry [5]. In numerous instances, mechanistic studies of chemical reactions using theoretical methods have achieve acceptable levels of accuracy and high computational speed [10, 11]. These theoretical approaches have demonstrated their capability to provide valuable insights into reaction mechanisms, even in complex systems, while offering the advantage of faster analysis compared to purely experimental methods. By evaluating potential reaction pathways and comparing their energies with experimental data, it is possible to propose a plausible mechanism for a reaction. Computational chemistry is a field within chemical science that utilizes mathematical and physical principles to solve chemical problems. It is employed to predict the structure of molecules, their inherent energy, and properties, as well as to study chemical reactions. Essentially, computational chemistry serves as a tool that allows for the investigation of chemical phenomena through theoretical means, without the need for practical laboratory experiments. By running computer programs, researchers can explore and analyze chemical phenomena theoretically. A computational method or model is a specific approach that involves a set of approximations combined with a computational algorithm. In the case of computational chemistry, atomic orbitals are inputted based on a chosen basis set to calculate molecular orbitals and energy, ultimately yielding information about energy levels and minimum energy [12–15]. In the mentioned research, computational chemistry has been utilized to support the proposed reaction mechanism for the synthesis of α-

cyanophosphonates. In general, phosphonates and their derivatives are classified as organophosphorus compounds, which are widely used in agricultural industries and have biological activity [16, 17]. Formulations containing phosphonates are used to control corrosion of carbon steel in cooling systems [18].

These compounds have good stability against heat and also in some industries can be used for extraction of metals. These compounds also have pharmaceutical properties [19, 20]. For example, Tenofovir is an antiviral drug that prevents the multiplication of viruses It prevents AIDS and hepatitis B in the body [21]. Fosfomycin is also an antibiotic used to treat infection Bladder is used [22]. Also, fosfidomycin is used in the treatment of malaria [23]. So far, only three synthetic methods of α-cyanophosphonates using β-nitrostyrenes have been reported. In one of these methods, by using the reaction between diethyl phosphite and beta-nitrostyrene, the compound diethyl (cyano (phenylmethyl)) phosphonate and the other product diethyl 1-phenyl vinyl phosphonate were synthesized at 150°C for two hours [24]. In another study, compound diethyl (cyano (phenylmethyl)) phosphonate was prepared using the reaction between diethyl (trimethylsilyl) sulfonate and beta-nitrostyrene [25] And finally, trimethyl phosphite was also used and the reaction of this compound with β-nitrostyrene led to the synthesis of compound dimethyl (cyano(methoxy)(phenyl) methyl) phosphonate [26]. However, in this project, in continuation of our previous theoretical studies [27, 28], we tried to investigate the formation mechanism of α-cyanophosphonates resulting from the reaction between triphenyl phosphite and β-nitrostyrenes through computational methods.

2. Computational

The calculations in this study were conducted using the Gaussian program, specifically version 09 [29]. GaussView 05 software was utilized to draw appropriate structures for the raw materials, intermediates, transition states, side products, and products. To optimize the molecules, the B3LYP/6-31G method was initially employed. Subsequently, the final calculations were performed using the M062X method, which is a subset of the density functional theory (DFT) method, along with the def2svp basis set. This method is one of the best DFT methods to study the reaction mechanism. all the raw materials, products, and reaction intermediates were optimized using this method and under basic conditions. The absence of negative frequency indicates that the compounds have reached their lowest energy level.

To obtain the transition states, the compounds were further optimized using the QST3 method. This involved utilizing the optimized structures of the starting material, the product, and the proposed structure of the transition state. The presence of a negative frequency confirmed the presence of a first-order saddle-shaped structure. Additionally, the "pop = full" keyword was used in the command line to examine the molecular orbital structure of substances and identify reactive sites. The absence of negative frequencies in the calculations indicates that the compounds are at their lowest energy level.

In the subsequent analysis, IEFPCM calculations will be employed to investigate the solvent effect. Finally, all frequency calculations, including energies, were appropriately corrected using conversion factors and then utilized for further analysis.

Various energies and thermodynamic data were extracted from the calculation output file, and correction coefficients were applied to eliminate inherent errors in the calculations. Thermodynamic data such as relative Gibbs free energy and relative electronic energy were used to assess the reaction path, while kinetic data such as rate constants were employed to examine the reaction kinetics. These data were converted to kcal/mol using energy conversion coefficients. The rate constants and thermodynamic equilibrium constants for each step were calculated using specific relationships and organized in tables. The rate constant as well as the thermodynamic equilibrium constant of each step were calculated using equations (1) and (2).

$K_{eq} = e^{(\frac{-\Delta G}{RT})}$) Equilibrium constant (Eq. 1)

$k = \frac{k_B T}{h} e^{\left(\frac{-\Delta G^{\ddagger}}{RT}\right)}$ rate constant (Eq. 2)

To estimate the level of molecular activity and using the HOMO and LUMO energy data, several valuable parameters such as hardness (η) (4), softness (s) (5), electronegativity index (ω) (6) and chemical potential (μ) (3) using equations 1–4 [30–32].

$\mu = \frac{(E_{LUMO}+E_{HOMO})}{2}$ (Eq. 3)

$\eta = \frac{(E_{LUMO}-E_{HOMO})}{2}$ (Eq. 4)

$S = \frac{1}{\eta}$ (Eq. 5)

$\omega = \frac{\mu^2}{2\eta}$ (Eq. 6)

3. Results and discussion

3.1 Proposed reaction mechanism of nitrostyrene with triphenyl phosphite

The available information suggests that there are potential mechanisms for this reaction, which are illustrated in Scheme 1. The synthesis of the resulting product is proposed to occur through three different routes, which will be thoroughly examined in the theoretical part of this research. In one of these routes, triphenyl phosphite is initially attached to the beta position of β-nitrostyrene, leading to the formation of the a1 ion pair through the ts1 transition state. The addition of nucleophiles to the beta position of an alkene containing an electron-withdrawing group is the most likely explanation that can be further investigated. Subsequently, the negatively charged oxygen in the intermediate a1 can interact with the positively charged phosphorus, resulting in the conversion of the ion-pair intermediate a1 into the neutral cyclic intermediate a2. This step, similar to the process observed in the Wittig reaction, has been extensively documented and verified. Following this, through rearrangement within the intermediate pentagonal ring a2 and by traversing the transition state ts2, the triphenyl phosphate group is eliminated from the compound, leading to the formation of the intermediate 2-nitrosovinylbenzene. Subsequently, another molecule of triphenyl phosphite is introduced to the beta position of 2-nitrosovinylbenzene, and by passing through the transition state ts3, the intermediate a4 is formed. Following that, a negatively charged oxygen is introduced to a positively charged phosphorus, resulting in the formation of intermediate a5. In the subsequent step, the phenoxy group separates the imine hydrogen and causes a rearrangement of the intermediate, leading to the formation of the α-cyanophosphonate product. However, based on the investigation of thermodynamic data, it was determined that the energy of intermediate a5 was not reasonable. Consequently, it was concluded that intermediate a4, which involves rearrangement and removal of phenol (bp3), is responsible for the formation of the final product. Despite extensive efforts, a suitable transition state for this particular step could not be identified. Another possible mechanism to consider (path b) involves adding the triphenyl phosphite molecule to the oxygen atom of the nitro group. This results in the formation of the intermediate ion pair b1. Subsequently, by adding a second molecule of triphenyl phosphite to the beta position of intermediate b1, triphenyl phosphate is eliminated, leading to the formation of intermediate a4. The subsequent steps along this pathway are similar to those observed in route a. The third mechanism pathway (c) involves enhancing the nucleophilicity of triphenyl phosphite towards the nitrogen of the nitro group in the initial step. Subsequently, by connecting the oxygen of

the nitro group to phosphorus, intermediate c2 is formed. This is followed by the formation of intermediate c3 through an intramolecular rearrangement. In the next step, by increasing the nucleophilicity of the second molecule of triphenyl phosphite towards the beta position of compound c3 and removing the phenoxy group, intermediate c4 is formed. Then, the phenoxy molecule reacts with triphenyl phosphate, resulting in the formation of intermediate a4 through a nucleophilic substitution on compound c4. It is important to note that the presence of two mmol of triphenyl phosphite is necessary for this reaction, and all three proposed mechanisms are designed accordingly. All three pathways of the proposed mechanism ultimately lead to the formation of intermediate a5. Additionally, triphenyl phosphate and phenol by-products are formed in all three pathways. In the subsequent step, due to the significantly higher energy of compound a5 compared to a4, a5 is disregarded, and it is concluded that a4 directly converts to the product without going through intermediate a5. This conversion involves the simultaneous removal of phenoxy from one side and separation of the beta hydrogen from the other side. Despite numerous attempts, calculations for the transition state of the conversion from a4 to the product were unsuccessful. Considering that the product was obtained with much lower energy than a4 and the challenges associated with calculating transition states involving multiple simultaneous transitions, the calculations were concluded at this stage. The optimized structures obtained from these calculations are depicted in Fig. 1.

3.1.1-evaluation of path a

Based on the explanations provided in this section, we will focus on interpreting step a of the mechanism described in previous section. Tables 1 and 2 present the relative energy values, as well as thermodynamic and kinetic data. From the data in Table 1, it is evident that in path a, an energy of 11.72 kcal/mol is required to initiate the reaction. By utilizing this energy to convert the raw materials into a2, an energy of 12.06 kcal/mol is released. It is important to note that according to the proposed mechanism, molecule a1 is initially designed for route a in this step. However, when comparing the relative Gibbs free energy and relative total energy values, it is observed that intermediate a2 is more stable than intermediate a1, with values of 4.43 and 12.06 kcal/mol, respectively. Therefore, in the first step, the raw materials directly transform into the a2 form. Calculations indicate that the intermediate of the a1 ion pair is less stable, and the connection of oxygen with a negative charge to phosphorus with a positive charge result in a more stable cyclic form, similar to the betaine intermediate in the Wittig reaction. Scheme 2 illustrates the designed intermediates a1, a2, and the direct mechanism of converting raw materials to a2 for route a. In the second stage of the conversion process from a2 to a3, there is an increase in the energy barrier. However, this stage also leads to the formation of more stable products. The conversion of a2 to a3 has the highest energy barrier and is considered the rate-determining step (RDS). Additionally, when comparing the relative stability energies of the cis and trans forms of the a3 molecule, it is determined that the trans form is more stable. To convert trans a3 to a4, an energy of 21.38 kcal/mol is required. Compound a5 is highly unstable, so it is disregarded, and it is concluded that a4 directly transforms into the final product without passing through a5 as an intermediate.

Table 1
values of relative free energy and relative electronic energy for path a

Rute a	relative G	relative E
Reactants	0	0
ts1	27.92	11.72
a2	4.43	-12.06
ts2	36.09	19.31
a3-t	-33.41	-33.92
ts3	2.4	-12.54
a4	-46.74	-63.29
P	-97.69	-99.61

Table 2
kinetic and thermodynamic data of path a

route a	ΔG	ΔG#	ΔE	BE	Keq	k
reactants to a1	31.85	27.92	15.83	11.72	1.94×10^{-5}	3.88×10^{-5}
reactants to a2	4.43	—	-12.06	—	1.81×10^{-3}	—
a1 to a2	-27.42	—	-27.89	—	9.31×10^{16}	—
–a2 to a3-c	-35.6	31.66	-19.8	31.37	1.07×10^{22}	1.88×10^{-7}
a2 to a3-t	-37.84	31.66	-21.86	31.37	2.61×10^{23}	1.88×10^{-7}
a3-c to a4	-15.57	33.57	-31.43	19.32	4.32×10^{9}	1.24×10^{-8}
a3-t to a4	-13.33	35.81	-29.37	21.38	1.77×10^{8}	5.08×10^{-10}
a4 to a5	130.13	—	143.74	—	2.95×10^{-81}	—
a4 to p	-50.95	—	-36.32	—	3.39×10^{31}	—

However, despite numerous attempts, it was challenging to determine a proposed transition state for this step, and the calculations failed to identify the transition state in the final stage of becoming a product. Ultimately, a highly stable product, p, with a total energy of -96.26 kcal/mol compared to the raw materials and intermediates, was obtained. The energy diagrams of path a in terms of relative Gibbs free energy and relative electron energy are shown in Figs. 2 and 3, respectively. Based on the information provided in Tables 1 and 2, as well as the diagrams in Figs. 2 and 3, this pathway involves the intermediates a2, a3-t, and a4, along with the transition states ts1, ts2, and ts3. The cumulative energy barrier for this pathway is calculated to be 19.31 kcal/mol, ultimately resulting in the formation of the desired product.

3.1.2-evaluation of path b

In the described process, as mentioned earlier, triphenyl phosphite can be added to the oxygen atom of the nitro group in r1, resulting in the formation of molecule b1. Subsequently, by adding another molecule of r2 to the beta position of b1, intermediate bp1 is formed. Step a leads to the formation of a4, and the remaining steps follow a similar pattern to step

a. Therefore, for calculations in this direction, it is necessary to optimize the b1 molecule and its corresponding transition state. Despite numerous attempts and the utilization of different methods such as B3LYP/6-31G and m062x with the def2svp basis set, we were unable to successfully optimize this compound. It is noteworthy that in all computational calculations, the output files consistently showed the isolation of triphenyl phosphite and the nitro oxygen of compound r1, resulting in the formation of triphenyl phosphate (bp1) and compound a3. This suggests that in this particular pathway, intermediate a4 is directly formed without the formation of intermediate b1, through the simultaneous addition of two molecules of triphenyl phosphite to the oxygen of the nitro group and the beta position of nitrostyrene. Alternatively, as depicted in scheme 3, the triphenyl phosphite molecule separates an oxygen atom from the nitro group, and upon removal of triphenyl phosphate, intermediate a3 is generated.

3-1-3 evaluation of path c

According to the proposed mechanism, triphenyl phosphite is suggested to be added to the nitrogen of the nitro group in the r1 molecule, resulting in the formation of intermediate c1 as previously mentioned. However, during the calculations, despite numerous attempts and the utilization of different methods with the def2svp base set, errors occurred, and the desired intermediate could not be obtained. Subsequently, the focus shifted towards optimizing the existing intermediates in this pathway, and successful optimization was achieved for c3 and c4 intermediates. However, intermediate c2 and the suggested transition states could not be obtained, similar to what was observed in path b, leading to the formation of the c3 molecule. Consequently, it is proposed that the starting material r1 directly transforms into c3, followed by the conversion of c3 into c4, and ultimately forming a4 through the transition state depicted in scheme 4. The reaction then proceeds similarly to path a. The relative electron energy for intermediates c3 and c4 is determined to be 2.18 and 69.8 kCal/mol, respectively. Additionally, the relative free energy for these intermediates is calculated as 15.76 and 88.78 kCal/mol, respectively. By comparing these data with the energy of other intermediates, it is evident that intermediates c3 and c4 are highly unstable species. Consequently, it is not feasible to proceed with the reaction through path c. Due to the complexity of the calculations associated with the respective transition states, we have refrained from calculating the transition states for this step. This decision is based on the fact that the energy of the intermediates does not allow the reaction to proceed in this manner.

3 – 2 atomic charges from NBO calculations

Using the output of NBO calculations, the atomic charges for each atom of the β-nitrostyrene molecule and also the atomic charges of the atoms of the triphenyl phosphite molecule were obtained, which are displayed in Tables 3 and 4, and in this way we will be able to distinguish Which atom in triphenyl phosphite will tend to bond with which atom in β-nitrostyrene. In the Figs. 4 and 5 atoms of each molecule are shown with numbers. Table 3 shows that in the β-nitrostyrene molecule, the most positive charge is for nitrogen atom number 18 in the nitro group of β-nitrostyrene, which value is 0.526, followed by hydrogen 13 (0.260), hydrogen 15 (0.237), hydrogens 11 and 6 (0.236), hydrogen 7 (0.235) and hydrogen 9 (0.234) have the highest positive charge. The most negative charge is for oxygen atom number 17 (-0.414), followed by oxygen atom number 16 (-0.396). After oxygen atoms, carbon atoms have the most negative atomic charges. Carbon 1 (-0.222), Carbon 10 (-0.219), Carbon 2 (-0.207), Carbon 3 (-0.191), Carbon 5 (-0.188), Carbon 12 (164/ -0), carbon 4 (-0.102) and carbon 14 (-0.093). In triphenyl phosphite molecule, phosphorus atom number 1 has the most positive atomic charge (1.650). The most negative atom in this composition is oxygen atom 2 (-0.836), followed by oxygen 4 (-0.832) and oxygen 3 (-0.830). But as we know, it is phosphorus that has a nucleophile character and can attack electrophiles because of the free electron pair on it. Of course, due to the connection of three oxygen groups and the creation of a positive charge on phosphorus, this nucleophilic property is much less than that of phosphines, but this less nucleophilic property increases the selectivity of this compound. In the triphenyl phosphite

molecule, the phosphorus atom with the highest positive charge is attracted to the negatively charged atoms of β-nitrostyrene. The most positively charged atom in β-nitrostyrene is nitrogen, but it cannot form a bond. Following nitrogen, the hydrogen atoms with the highest positive charges are potential candidates for bonding. However, the negatively charged carbon atoms in the ring are unable to form bonds due to strong bonding forces. Only the oxygen atoms and carbon atoms 12 and 14 have the possibility of forming connections. Among these options, the oxygen atoms have the most negative charge, indicating a higher likelihood of forming a bond. Therefore, it can be concluded that the reaction is more likely to proceed through path b. Between carbon atoms 12 and 14, carbon 12 has a higher probability of forming a connection due to its more negative charge.

Table 3
atomic charges extracted from NBO calculations in the β-nitrostyrene molecule

number	atom	charge	Number	atom	Charge
1	C	-0.222	10	C	-0.219
2	C	-0.207	11	H	0.236
3	C	-0.191	12	C	-0.164
4	C	-0.102	13	H	0.260
5	C	-0.188	14	C	-0.093
6	H	-0.236	15	H	0.237
7	H	0.235	16	O	-0.396
8	H	0.229	17	O	-0.414
9	H	0.234	18	N	0.526

Table 4
Atomic charges extracted from NBO calculations on the triphenyl phosphite molecule

Number	atom	charge	number	atom	charge	number	atom	charge	number	atom	charge
1	P	1.650	10	C	-0.244	19	C	-0.213	28	H	0.240
2	O	-0.836	11	C	-0.211	20	C	-0.244	29	H	0.232
3	O	-0.830	12	C	-0.278	21	C	-0.210	30	H	0.231
4	O	-0.832	13	C	-0.264	22	C	-0.292	31	H	0.232
5	C	-0.316	14	C	-0.212	23	C	0.240	32	H	0.240
6	C	-0.320	15	C	-0.247	24	H	0.231	33	H	0.244
7	C	-0.326	16	C	-0.206	25	H	0.230	34	H	0.233
8	C	-0.263	17	C	-0.299	26	H	0.231	35	H	0.232
9	C	-0.217	18	C	-0.261	27	H	0.256	36	H	0.232

3–3 Investigating the role of solvent and comparing energy in different solvents

Although most modeling methods consider the behavior of molecules in the gas phase during calculations, in practical chemical processes, the majority of reactions occur in a solvent environment. Therefore, the interaction between the

desired compound and the solvent is significant, and different solvents can have varying effects on the reaction rate and progress, depending on their polarity and dielectric constant. In this research, three solvents, namely methanol, N,N-dimethylformamide, and water, were utilized. The widely used SCRF model, specifically the polarizable continuum PCM method, was employed to account for the solvent's free energy and calculate the corresponding thermodynamic parameters. To achieve this, the Hartree-Fock energy of all molecules was initially determined. Then, the total electron energy of the solvent was calculated by comparing the Hartree-Fock energy in the solvent phase with that in the gas phase. Subsequently, the total electron energy of the solvent was combined with the relative Gibbs free energy data and the relative electron energy of all species in the gas phase. This allowed for the calculation of the relative Gibbs free energy and relative electron energy data in the three solvents. The relative Geiss free energy and relative electron energy data were calculated in three solvents and are shown in Tables 5, 7 and 9. The thermodynamic data for path A in the three solvents are presented in Tables 6,8 and 10 and the diagrams of energy are shown in Figs. 6 to 11.

Table 5
relative Gibbs free energy data and total electronic energy in water solvent

Molecule	relative G	relative E	molecule	relative G	relative E
Reactants	0	0	a3-c	-30.93	-31.42
ts1	28.27	12.4	ts3	2.3	-11.94
a2	5.51	-10.97	a4	-46.27	-62.82
ts2	37.54	20.75	a5	-4.4	-7.34
a3-t	-33.98	-34.5	p	-98.18	-100.18

Table 6
thermodynamic and kinetic data of path a in water solvent

Reaction stage	ΔG	$\Delta G^{\#}$	ΔE	BE	Keq	k
reactants to a1	28.19	28.27	12.18	12.4	3.59×10^{-18}	2.35×10^{-5}
reactants to a2	5.51	—	-10.97	—	3.89×10^{-4}	—
a1 to a2	-22.68	—	-23.15	—	1.08×10^{14}	—
a2 to a3-c	-36.44	32.03	-20.45	31.72	3.55×10^{22}	1.11×10^{-7}
a2 to a3-t	-39.49	32.03	-23.53	31.72	2.74×10^{24}	1.11×10^{-7}
a3-c to a4	-15.34	33.23	-31.4	19.48	3.11×10^{9}	2.01×10^{-8}
a3-t to a4	-12.29	36.28	-28.32	22.56	4.03×10^{7}	2.60×10^{-10}
a4 to a5	41.87	—	55.48	—	1.23×10^{-26}	—
a4 to p	-51.91	—	-37.36	—	1.33×10^{32}	—

Table 7
relative Gibbs free energy data and total energy in methanol solvent

Molecule	relative G	relative E	molecule	relative G	relative E
Reactants	0	0	a3-c	-30.94	-31.63
ts1	28.27	12.4	ts3	3	-11.94
a2	5.53	-10.94	a4	-46.26	-62.82
ts2	37.54	20.76	a5	-2.7	-5.64
a3-t	-33.97	-34.49	P	-98.06	-100.06

Table 8
thermodynamic and kinetic data of path a in methanol solvent

Reaction stage	ΔG	$\Delta G^{\#}$	ΔE	BE	Keq	k
reactants to a1	28.33	28.27	12.31	12.4	2.94×10^{-18}	2.35×10^{-5}
reactants to a2	5.53		-10.94		3.78×10^{-4}	
a1 to a2	-22.8		-23.25		1.29×10^{14}	
a2 to a3-c	-36.47	32.01	-20.69	31.7	3.71×10^{22}	1.14×10^{-7}
a2 to a3-t	-39.5	32.01	-23.55	31.7	2.78×10^{24}	1.14×10^{-7}
a3-c to a4	-15.32	33.94	-31.19	19.69	3.02×10^{9}	7.30×10^{-9}
a3-t to a4	-12.29	36.97	-28.33	22.55	4.03×10^{7}	9.73×10^{-11}
a4 to a5	43.56		57.18		1.10×10^{-27}	
a4 to p	-51.8		-37.24		1.14×10^{32}	

Table 9
relative Gibbs free energy data and total energy in N, N-dimethylformamide solvent

Molecule	relative G	relative E	molecule	relative G	relative E
Reactants	0	0	a3-c	-30.94	-31.63
ts1	28.27	12.4	ts3	3	-11.94
a2	5.53	-10.95	a4	-46.26	-62.81
ts2	37.54	20.76	a5	-3.06	-6
a3-t	-33.97	-34.49	P	-98.08	-100.08

Table 10
thermodynamic and kinetic data of path a in N, N-dimethyformamide solvent

Reaction stage	ΔG	ΔG#	ΔE	BE	Keq	K
reactants to a1	28.3	28.27	12.28	12.4	3.07×10^{-18}	2.35×10^{-5}
reactants to a2	5.53		-10.95		3.78×10^{-4}	
a1 to a2	-22.77		-23.23		1.23×10^{14}	
a2 to a3-c	-36.47	32.01	-20.68	31.71	3.71×10^{22}	1.14×10^{-7}
a2 to a3-t	-39.5	32.01	-23.54	31.71	2.78×10^{24}	1.14×10^{-7}
a3-c to a4	-15.32	33.94	-31.18	19.69	3.02×10^{9}	7.30×10^{-9}
a3-t to a4	-12.29	36.97	-28.32	22.55	4.03×10^{7}	9.73×10^{-11}
a4 to a5	43.2		56.81		1.84×10^{-27}	
a4 to p	-51.82		-37.27		1.17×10^{32}	

3-3-1 Solvent role in evaluating the proposed path a

Based on the data obtained, it is evident that the relative changes in free energy for the initial step, specifically the addition of triphenyl phosphite to β-nitrostyrene and the formation of intermediate a2, are nearly identical in all three solvents, amounting to 5.53 kcal/mol. However, when compared to the gas phase, there is an increase of approximately 1.1 kcal/mol. The total electronic energy remains relatively consistent across all three solvents, approximately − 10.95 kcal/mol, with a similar increase of 1.1 kcal/mol compared to the gas phase. This suggests that this particular stage is less favorable in the solvent phase compared to the gas phase. In contrast, the relative changes in free energy during the second step, specifically the conversion from a2 to a3-t, are consistent across all three solvents, measuring at -39.50 kcal/mol. However, compared to the gas phase, each solvent exhibits a more negative change of 1.66 kcal/mol. The overall electron energy changes during the conversion from intermediate a2 to intermediate a3-t are nearly identical in all three solvents, amounting to -23.55 kcal/mol. This value is approximately 1.69 kcal/mol more negative than the gas phase, indicating that this step of route a is more efficiently carried out in a solvent. The Gibbs free energy changes in the third step, involving the conversion of intermediate a3-t to a4, remain consistent across all three solvents at -12.29 kcal/mol. This value is 1.04 kcal/mol higher than the gas phase. Similarly, the total electron energy changes during this phase are also consistent in all three solvents, measuring at -28.33 kcal/mol. This value is 1.04 kcal/mol higher than the gas phase, suggesting that this phase is less favorable in a solvent compared to the gas phase. In the last step, which entails the conversion of intermediate a4 to the final product, the Gibbs free energy changes in all three solvents exhibit a more negative value of approximately 0.96 kcal/mol compared to the gas phase. Additionally, the total electron energy changes in all three solvents are approximately one kcal/mol more negative than the gas phase. These observations indicate that this stage is more favorable in a solvent compared to the gas phase. The comparison of the relative free energy of the product in the gas phase (-69.97 kcal/mol) and in the solvent phase (-98.08 kcal/mol) reveals that the product becomes more stable in the presence of a solvent, with an increase of approximately 0.4 kcal/mol compared to the gas phase. This suggests that the solvent has a significant impact on the thermodynamic stability of the system. Notably, the stability of intermediate a5 shows a substantial increase in the solvent phase compared to the gas phase. However, there is not a significant difference in energy among water, methanol, and dimethylformamide solvents.

3-3-2 Solvent role in evaluating the proposed path b

Path b refers to a single-step process where triphenyl phosphite is added to the oxygen atom of the nitro group in β-nitrostyrene. This results in the formation of a3-t and triphenyl phosphate. The conversion of the starting materials to a3-t is driven by the decrease in Gibbs free energy. In the gas phase, the relative Gibbs free energy of a3-t is -41.33 kcal/mol, while in all three solvent phases, it is approximately − 33.97 kcal/mol. This indicates that the Gibbs free energy has become more negative by about − 0.56 kcal/mol in the solvent phase. The total electron energy of this intermediate in the gas phase is calculated to be -33.92 kcal/mol, which decreases to approximately − 34.50 kcal/mol in the solvent phase. This change indicates that path b is relatively more favorable in the solvent phase compared to the gas phase.

3-3-3 Solvent role in evaluating the proposed path c

Since the optimization of structures for c1, c2, and all states in path c was unsuccessful, our focus was on comparing the energy of intermediates c3 and c4 in different phases: gas phase, water solvent, methanol solvent, and N, N-dimethylformamide solvent. The relative Gibbs free energy values for intermediate c3 were calculated as 15.76 kcal/mol in the gas phase and 15.59 kcal/mol in water solvent. In methanol solvent, the values were 15.62 kcal/mol, and in n,n-dimethylformamide solvent, they were 15.61 kcal/mol. Additionally, the total electron energy for intermediate c3 was determined as 2.19 kcal/mol in the gas phase, 2.02 kcal/mol in water solvent, 2.05 kcal/mol in methanol solvent, and 2.05 kcal/mol in n,n-dimethylformamide solvent. These results indicate that the stability of this intermediate is increased by approximately 0.17 kcal/mol in the solvent phase compared to the gas phase.

3–4 evaluation of reactivity parameters and calculations of molecular orbitals

Initially, the energy levels of the Highest Occupied Molecular Orbital (HOMO) and Lowest Unoccupied Molecular Orbital (LUMO) were computed, and the shape of these orbitals for all molecules is provided in Fig. 12. In the case of triphenyl phosphite acting as a nucleophile, the electrons in its HOMO orbital are added to the LUMO orbitals in β-nitrostyrene, resulting in bond formation. To assess the reactivity of the atoms, the contributions of their respective LUMO orbitals were separately compared. These findings are presented in Table 11. Upon analysis, it was observed that the total contribution of LUMO atomic orbitals for the β carbon (0.6785) exceeds that of the α carbon (-0.51868) when performing pop = full calculations. Consequently, the β carbon exhibits a higher propensity for nucleophilic attack and displays greater reactivity. Therefore, the HOMO orbital of triphenyl phosphite is connected to the LUMO orbital of the β carbon in β-nitrostyrene. And after that, the most atom that has a chance of nuclear attack is the oxygen atom. As a result, the HOMO orbital of triphenyl phosphite is connected to the LUMO orbital of β-carbon in β-nitrostyrene. According to these data, it is clear that the chance that the reaction from the C path, i.e., the addition of phosphorus to the nitrogen atom in β-nitrostyrene, is very low. Based on the information provided in Table 12, the energy gap for triphenyl phosphite is 0.296 ev, while for β-nitrostyrene it is 0.245 ev. This indicates that the energy gap is higher for triphenyl phosphite, making it harder. The hardness values for triphenyl phosphite and β-nitrostyrene are 0.148 and 0.123, respectively. The softness values for these compounds are calculated as 6.751 and 8.150 ev, respectively. These values are not significantly different from each other, which suggests that a reaction between them is possible. The LUMO orbital energy values for the molecules r1, a3-t, and c2, which act as electrophiles, are calculated as -0.064, -0.069, and − 0.080 ev, respectively. The LUMO energy value for triphenyl phosphite, acting as a nucleophile, is positive at 0.011 ev. The electrophilic value for β-nitrostyrene is 0.002 ev, which is considered an acceptable value for carrying out the reaction. Based on the provided comparison of hardness and softness data between molecules a1 and a2, it can be observed that the hardness of molecule a2 (with an intermediate hardness of 0.143 ev) is higher than that of a1 (with an intermediate hardness of 0.111 ev). Additionally, the softness of a2 (with an intermediate softness of 0.147 ev) is lower compared to a1 (with a softness of 0.9031 ev). These findings indicate that intermediate a2 is more stable than a1. The hardness values for

intermediates a3-t and a3-c are both 0.112 ev, and their softness levels are calculated as 8.910 ev. The potential energy data in the table further support the stability of the a2 structure compared to the a1 structure. This is because the a2 intermediate has a lower chemical potential energy (-0.136 ev) compared to the a1 intermediate (-0.121 ev). The potential energy values for the trans and cis a3 intermediates are − 0.177 and − 0.181 ev, respectively. Based on the provided information, the energy gaps of intermediates c3 and c4 are calculated as 0.171 and 0.228 ev, respectively. Comparing these values with the intermediates of path a, it can be concluded that c3 and c4 are more reactive species. The softness values for these species are calculated as 11.712 and 8.760 ev, respectively, indicating higher softness and increased reactivity. The energy gap for the final product compound is calculated as 0.307 ev, which is higher than the energy gaps of the raw materials and intermediates. This suggests that the final product is harder and more stable. Additionally, the softness of the final product is 6.512 ev, which is lower than that of other species, indicating lower reactivity. The chemical potential of the final product compound is -0.152, which is considered an acceptable value for the stability of the compound.

Table 11
The total contribution of LUMO orbitals in nitrogen.
oxygens 16, 17 and carbons 12 and 14, of β-nitrostyrene

Carbons	Total contribution of LUMO orbitals
Carbon 12 (β)	0.6785
Carbon 14 (α)	-0.51868
Nitrogen	0.02442
Oxygen 16	0.47377
Oxygen 17	0.42372

Table 12
HOMO, LUMO energy level, hardness, softness, electronegativity index and chemical potential data of compounds

	r1	r2	bp1	bp2	a1	a2	a3-t	a3-c
HOMO	-0.311	-0.285	-0.299	-0.036	-0.232	-0.278	-0.290	-0.293
LUMO	-0.064	0.011	0.011	0.217	-0.011	0.007	-0.065	-0.069
Eg	0.247	0.296	0.310	0.253	0.221	0.285	0.224	0.224
μ	-0.187	-0.137	-0.144	0.091	-0.121	-0.136	-0.177	-0.181
η	0.124	0.148	0.155	0.127	0.111	0.143	0.112	0.112
s	8.089	6.751	6.457	7.891	9.031	7.014	8.911	8.910
ω	0.002	0.001	0.002	0.001	0.001	0.001	0.002	0.002
	a4	a5	c3	c4	p	ts1	ts2	ts3
HOMO	-0.269	-0.421	-0.251	-0.388	-0.305	-0.231	-0.252	-0.255
LUMO	0.008	-0.141	-0.080	-0.160	0.002	-0.005	-0.086	-0.061
Eg	0.278	0.280	0.171	0.228	0.307	0.227	0.166	0.194
μ	-0.130	-0.281	-0.166	-0.274	-0.152	-0.118	-0.169	-0.158
η	0.139	0.140	0.085	0.114	0.154	0.113	0.083	0.097
s	7.205	7.146	11.712	8.760	6.512	8.823	12.034	10.313
ω	0.001	0.006	0.001	0.004	0.002	0.001	0.001	0.001

Conclusion

DFT calculations were used to investigate the reaction mechanism. According to the position of addition of triphenyl phosphite as a nucleophile to beta-nitrostyrene, three mechanisms were proposed for the reaction. According to the pop = full calculations, it was found that among nitrogen atoms, oxygen and carbons 12 and 14 of beta-nitrostyrene, carbon 12 has a higher lumo contribution and is more reactive than other atoms. And then oxygen has a greater contribution. Considering these cases, as well as the lack of success in optimizing c1, c2 intermediates in path c, and the higher relative Gibbs free energy value of c3, c4 intermediates compared to the intermediates of path a, the probability that the reaction will go through path c decreases. In route b, intermediate b1 was not optimized, but according to the final result of optimization in this route, it was found that by adding triphenyl phosphite to β-nitrostyrene, the oxygen of β-nitrostyrene was removed at the same time, and the products a3-t and triphenyl phosphate were created. which indicates that the number of intermediates in this route has decreased.

According to the solvent calculations that were done in three different solvents, water, methanol, and N,N-dimethylformamide, the results indicated that the energy changes in all routs were very similar in all three solvents, but some phases were slightly different from the gas phase. The relative Gibbs energy changes of the RDS step in all three solvents are the same, but compared to the gas phase, it is about 1.66 kcal/mol more negative, which indicates that this step is faster in the solvent. also, by comparing the relative Gibbs energy data and the total electronic energy of the product in solvents with the gas phase, it was concluded that the product was more stable in these three solvents.

Declarations

Acknowledgment

All calculations were done using the services provided by National HighPerformance Computing Center (NHPCC) at Isfahan University of Technology (IUT).

Ethical Approval

This work does not include any human and/ or animal studies.

Competing interests

The Authors declare that there is no financial or personal interest.

Authors' contributions

H. T. designed the study, and corrected the manuscript. S. S. performed all calculations, extracted and analysed all data, prepared figures, tables, and scheme.A. M. wrote the manuscript draft.

Funding

No fund is received for this work.

Availability of data and materials

All data are available and could be sent on request from the corresponding author.

References

1. Y. M. Sun, H. Y. Zhang, D. Z. Chen, C. B. Liu, Org. Lett. *4*(17), 2909-2911 (2002)
2. T. Ziegler, J. Autschbach., *105*(6), 2695-2722 (2005). 1. B. J. McClelland, Chem. Rev. 64(3), 301-315 (1964)
3. W. Notz, F., Tanaka,C. F. Barbas, Acc. Chem. Res. *37*(8), 580-591 (2004)
4. N. L. Holy, J. D. Marcum, Angew. Chem., Int. Ed. Engl. 10(2), 115-124(1971)
5. H. Tavakol, M. A. Ranjbari, A. Mahmoudi, Comput Theor Chem. *1154*, 37-43 (2019)
6. I. B. Obot, S. Kaya, C. Kaya, B. Tüzün, Res. Chem. Intermed. *42*, 4963-4983 (2016)
7. I. B. Obot, N. O. Obi-Egbedi, E. E. Ebenso, A. S. Afolabi, E. E Oguzie, Res. Chem. Intermed. *39*, 1927-1948 (2013)
8. M. Nikpassand, L. Z. Fekri, P. N. Rahro, Res. Chem. Intermed. *45*, 1707-1719 (2019)
9. A. Bhan, Y. V. Joshi, W. N. Delgass, K. T. Thomson, J. Phys. Chem. B. *107*(38), 10476-10487 (2003)
10. X. Rozanska, R. A. van Santen, T. Demuth, F. Hutschka, J. Hafner, J. Phys. Chem. B. *107*(6), 1309-1315 (2003)
11. D.C. Young, Comput. Chem. (2001)
12. F. Roncaroli, M. E. Ruggiero, D. W. Franco, G. L. Estiú, J. A. Olabe, Inorg. Chem. *41*(22), 5760-5769 (2002)
13. Á. Madarász, Z. Dósa, S. Varga, T. Soós, A. Csámpai, I. Pápai, ACS Catal. *6*(7), 4379-4387 (2016)
14. J. E. Lee, W. Choi, B. J. Mhin, J. Phys. Chem. A. *107*(15), 2693-2699 (2003)
15. K. Zhu, P. D. Achord, X. Zhang, K. Krogh-Jespersen, A. S Goldman, J. Am. Chem. Soc. *126*(40), 13044-13053 (2004)
16. N. Hazeri, M. T. Maghsoodlou, S. M. Habibi-Khorassani, J. Aboonajmi, M. Lashkari, S. S. Sajadikhah, Res. Chem. Intermed. *40*, 1781-1788 (2014)

17. M. H. Shaikh, D. D. Subhedar, F. A. Kalam Khan, J. N. Sangshetti, B. B. Shingate, Res. Chem. Intermed. *42*, 5115-5131 (2016)
18. D. Sarada Kalyani, S. Srinivasa Rao, M. Sarath Babu, B. V. Appa Rao, B. Sreedhar, Res. Chem. Intermed. *41*, 5007-5032 (2015)
19. C. Lopin, G. Gouhier, A. Gautier, S. R. Piettre, J. Org. Chem *68*(26), 9916-9923 (2003)
20. C. M. Sevrain, M. Berchel, H. Couthon P. A., Jaffrès, Beilstein J. Org. Chem. *13*(1), 2186-2213 (2017)
21. E. De Clercq, *Expert Rev Anti Infect Ther 1*(1), 21-43 (2003)
22. M. E. Falagas, E. K. Vouloumanou, G. Samonis, K. Z. Vardakas, Clin. Microbiol. Rev. *29*(2), 321-347 (2016)
23. E. I. Parkinson, A. Erb, A. C. Eliot, K. S. Ju,W. W. Metcalf, Nat. Chem. Biol. *15*(11), 1049-1056 (2019)
24. G. A. Russell, C. F. Yao, H. I. Tashtoush, J. E. Russell, D. F. Dedolph, J. Org. Chem. *56*(2), 663-669 (1991)
25. D. Y. Kim, D. Y. Oh, Synth. Commun. *17*(8), 953-957 (1987)
26. W. E. Krueger, J. R. Maloney, J. Org. Chem. *38*(24), 4208-4209 (1973)
27. H. Tavakol, P. Shafieyoon, Res. Chem. Inermed. 49, 3645–3658 (2023)
28. Z. Emami-Meibodi, H. Tavakol, K. Eskandari, Res. Chem. Inermed. 49, 3205–3225 (2023)
29. Gaussian 09, Revision B.01, Frisch, M. J.; Trucks, G. W.; Schlegel, H. B.; Scuseria, G. E.; Robb, M. A.; Cheeseman, J. R.; Scalmani, G.; Barone, V.; Petersson, G. A.; Nakatsuji, H.; Li, X.; Caricato, M.; Marenich, A. V.; Bloino, J.; Janesko, B. G.; Gomperts, R.; Mennucci, B.; Hratchian, H. P.; Ortiz, J. V.; Izmaylov, A. F.; Sonnenberg, J. L.; Williams-Young, D.; Ding, F.; Lipparini, F.; Egidi, F.; Goings, J.; Peng, B.; Petrone, A.; Henderson, T.; Ranasinghe, D.; Zakrzewski, V. G.; Gao, J.; Rega, N.; Zheng, G.; Liang, W.; Hada, M.; Ehara, M.; Toyota, K.; Fukuda, R.; Hasegawa, J.; Ishida, M.; Nakajima, T.; Honda, Y.; Kitao, O.; Nakai, H.; Vreven, T.; Throssell, K.; Montgomery, J. A., Jr.; Peralta, J. E.; Ogliaro, F.; Bearpark, M. J.; Heyd, J. J.; Brothers, E. N.; Kudin, K. N.; Staroverov, V. N.; Keith, T. A.; Kobayashi, R.; Normand, J.; Raghavachari, K.; Rendell, A. P.; Burant, J. C.; Iyengar, S. S.; Tomasi, J.; Cossi, M.; Millam, J. M.; Klene, M.; Adamo, C.; Cammi, R.; Ochterski, J. W.; Martin, R. L.; Morokuma, K.; Farkas, O.; Foresman, J. B.; Fox, D. J. Gaussian, Inc., Wallingford CT, 2016.
30. H. Tavakol, M. A. Ranjbari, M. T. Jafari-Chermahini, React. Kinet. Mech. Catal. *128*, 629-643 (2019)
31. H. Tavakol, H. Haghshenas, *Quantum Reports*, *3*(3), 366-375 (2021)
32. M. Bursch, J. M. Mewes, A. Hansen, S. Grimme, Angew. Chem., Int. Ed. Engl. *61*(42), (2022)

Schemes

Schemes 1-4 are available in the Supplementary Files section.

Figures

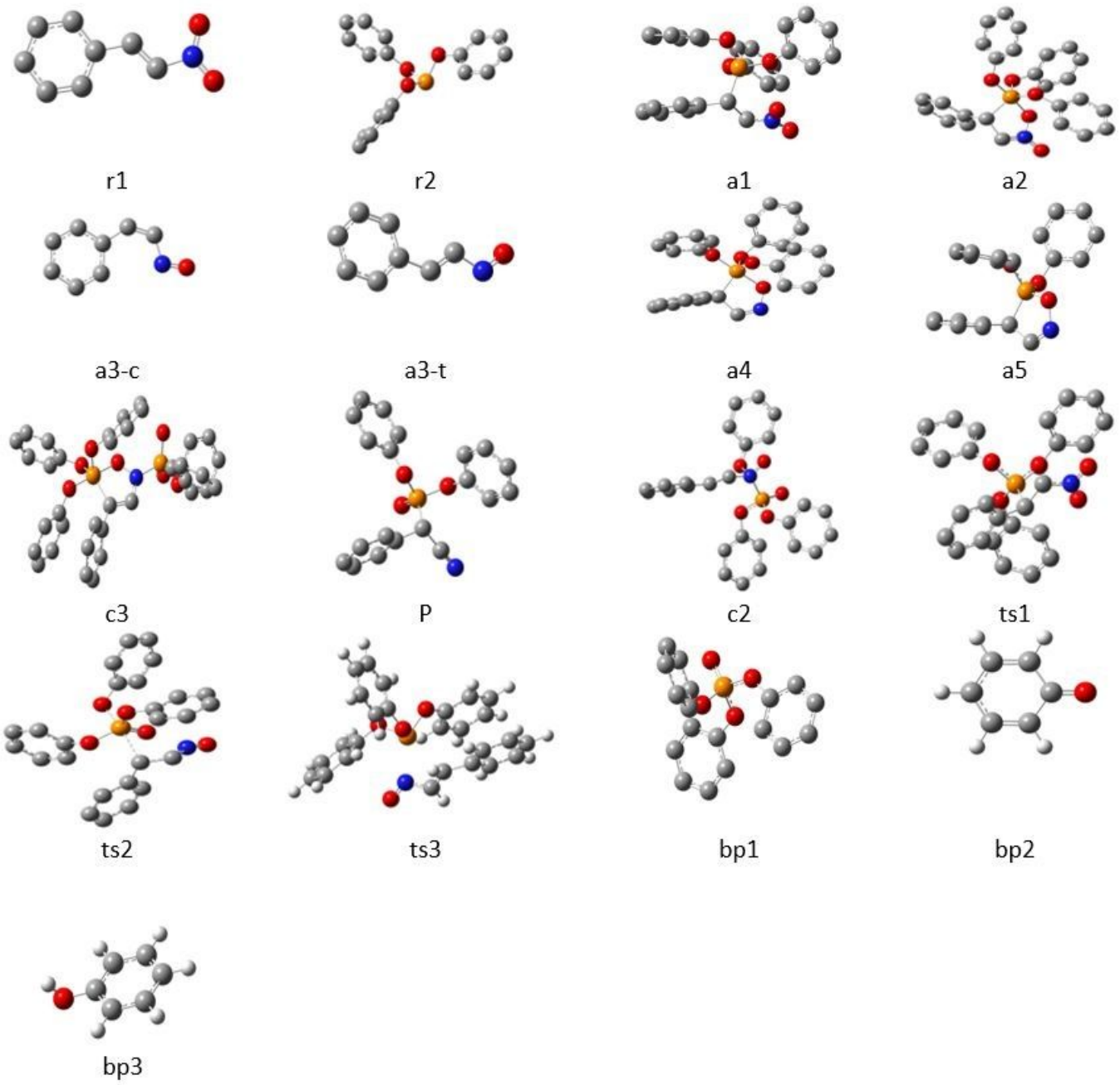

Figure 1

Optimized structure of compounds participating in the reaction

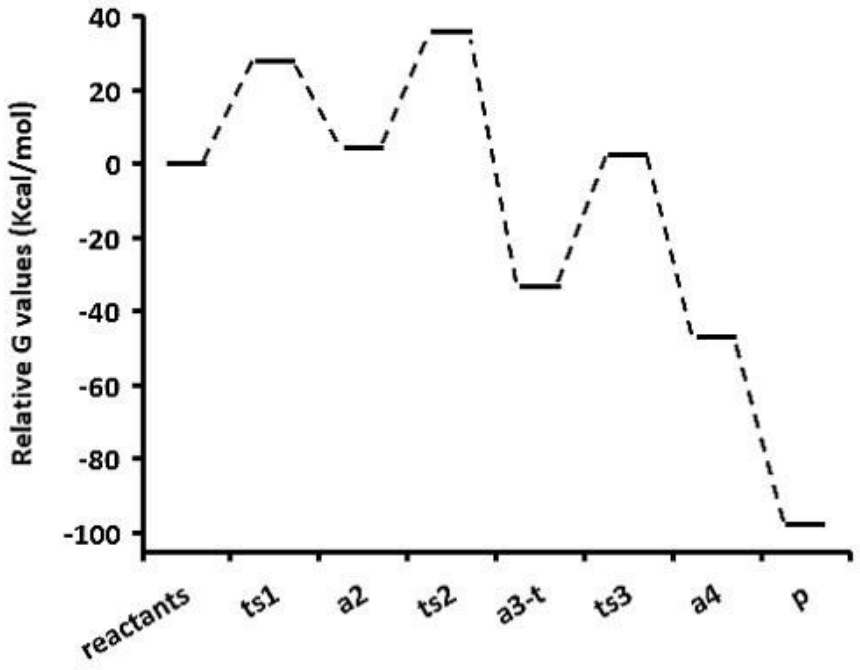

Figure 2

Gibbs relative free energy diagram of path a

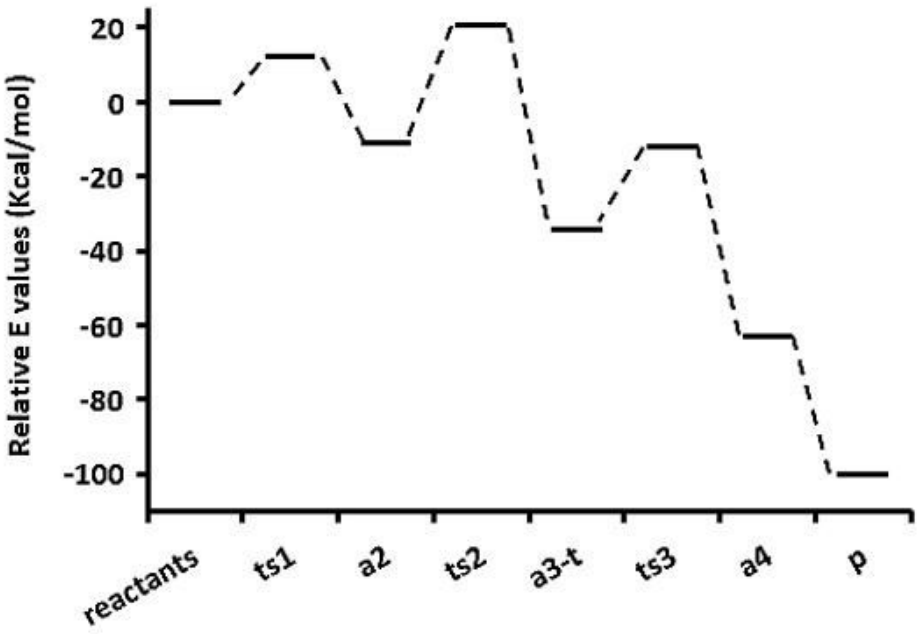

Figure 3

Diagram of electronic energy in path a

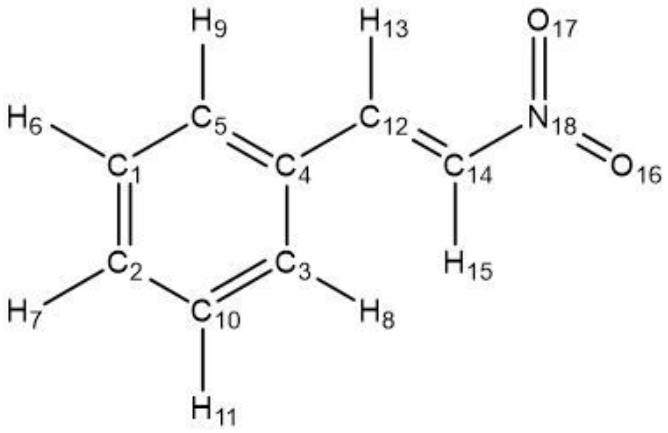

Figure 4

Structure of β-nitrostyrene with atom numbers

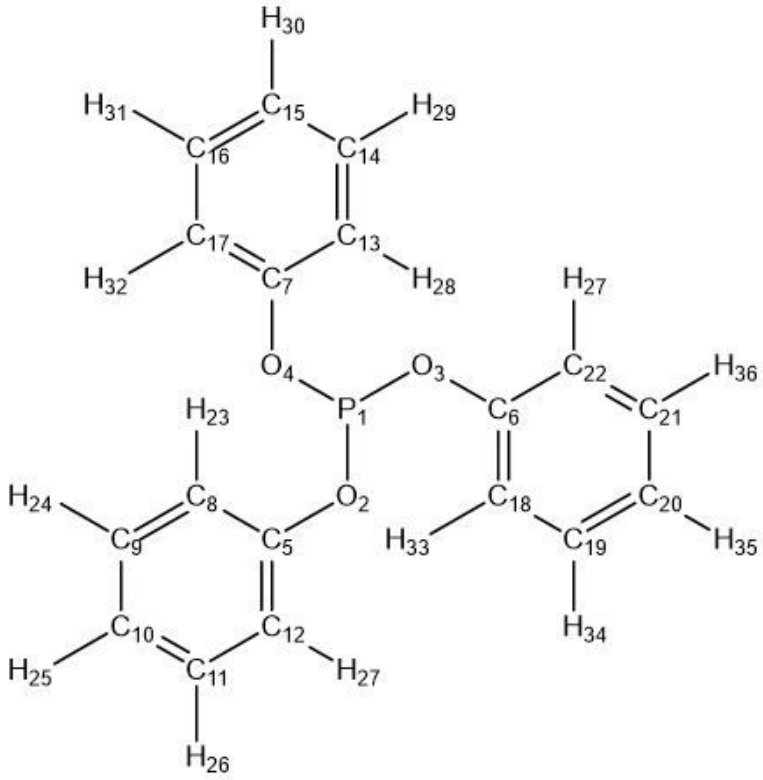

Figure 5

Structure of triphenyl phosphite with atomic numbers

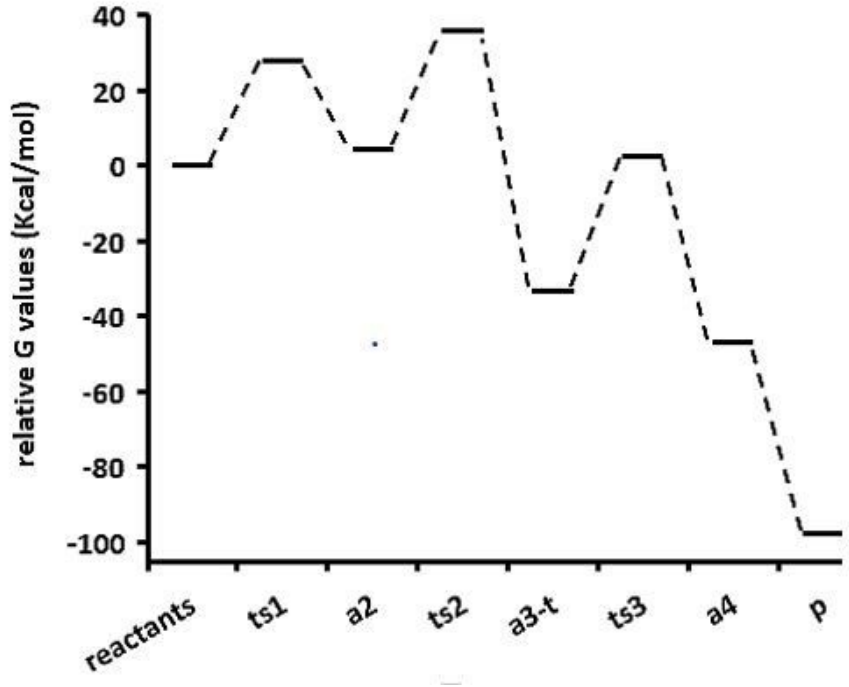

Figure 6

Gibbs relative free energy diagram of path ain water solvent

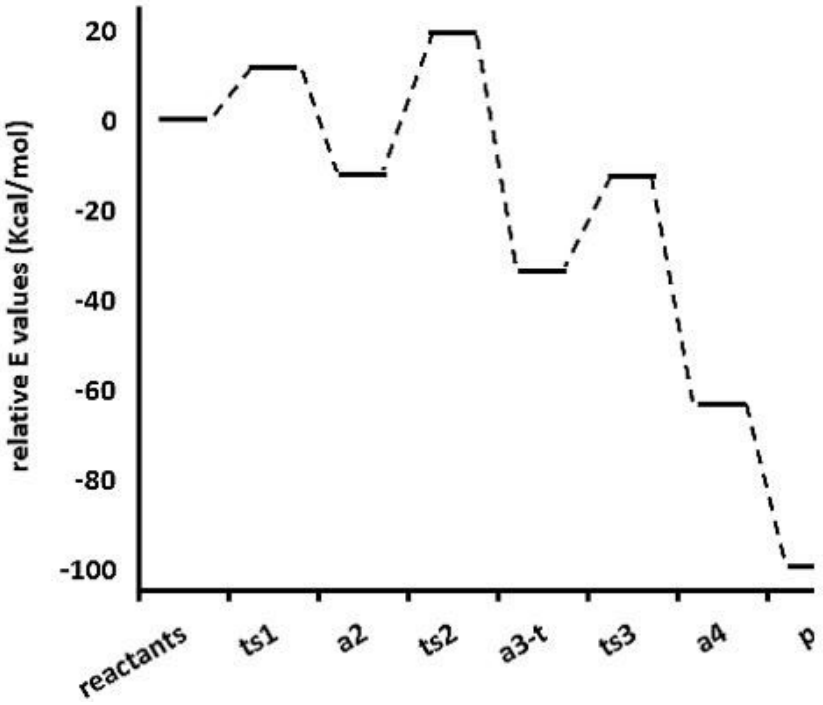

Figure 7

Diagram of electronic energy in path a in water solvent

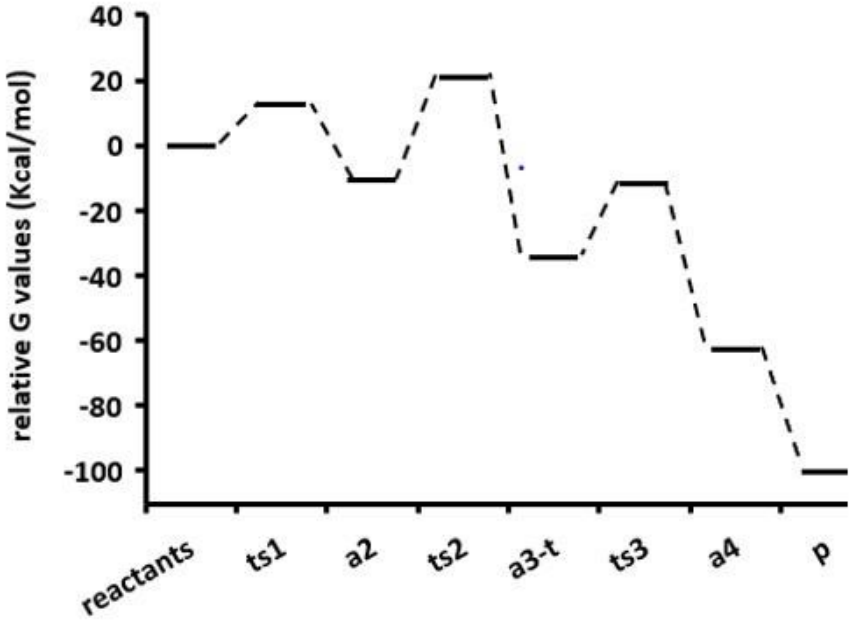

Figure 8

Gibbs relative free energy diagram of path ain methanol solvent

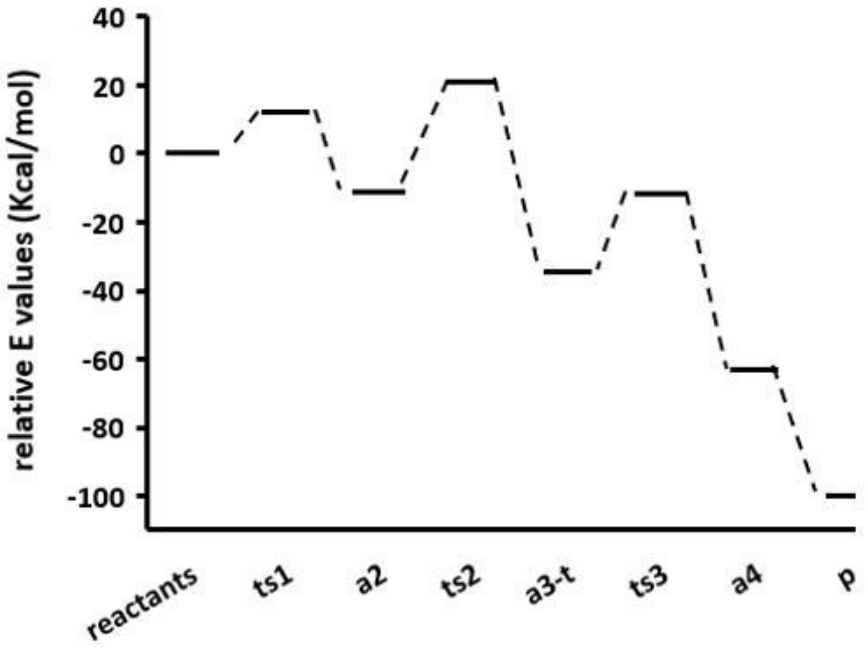

Figure 9

Diagram of electronic energy in path a in methanol solvent

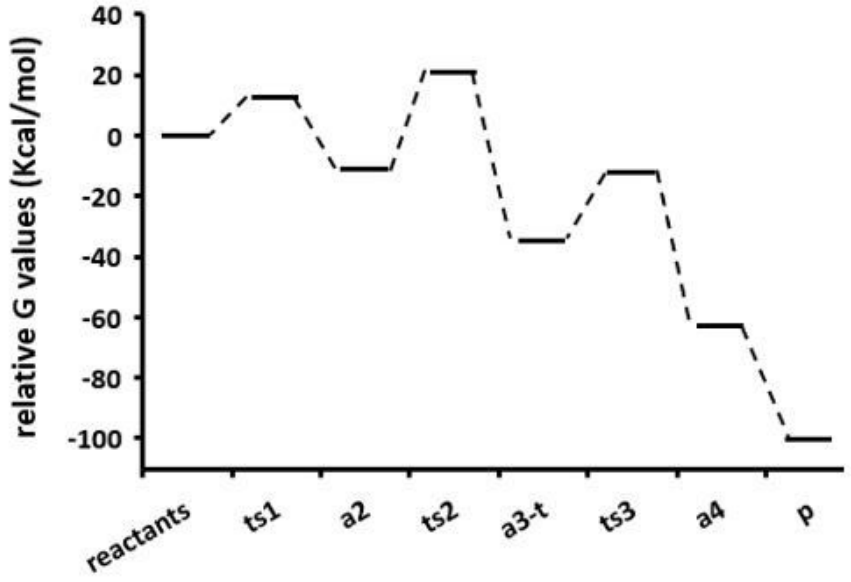

Figure 10

Gibbs relative free energy diagram of path a in N, N-dimethylformamide solvent

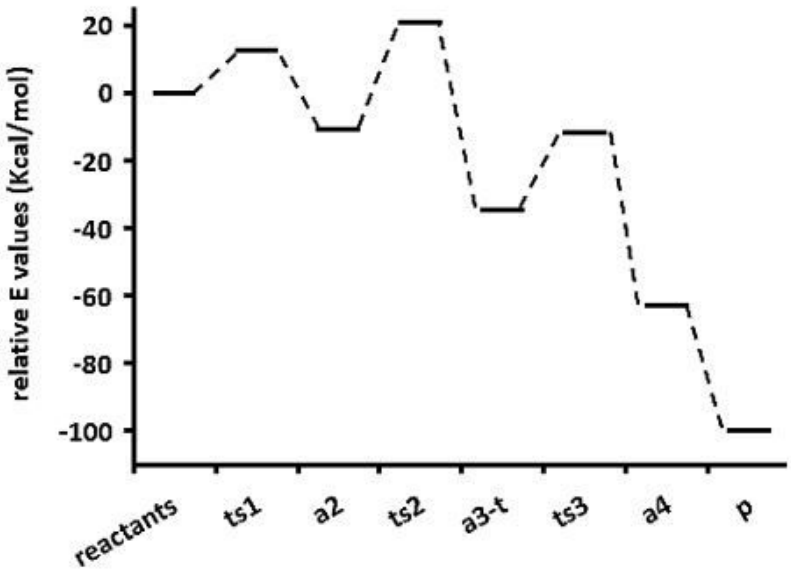

Figure 11

Diagram of electronic energy in path a in N, N-dimethylformamide solvent

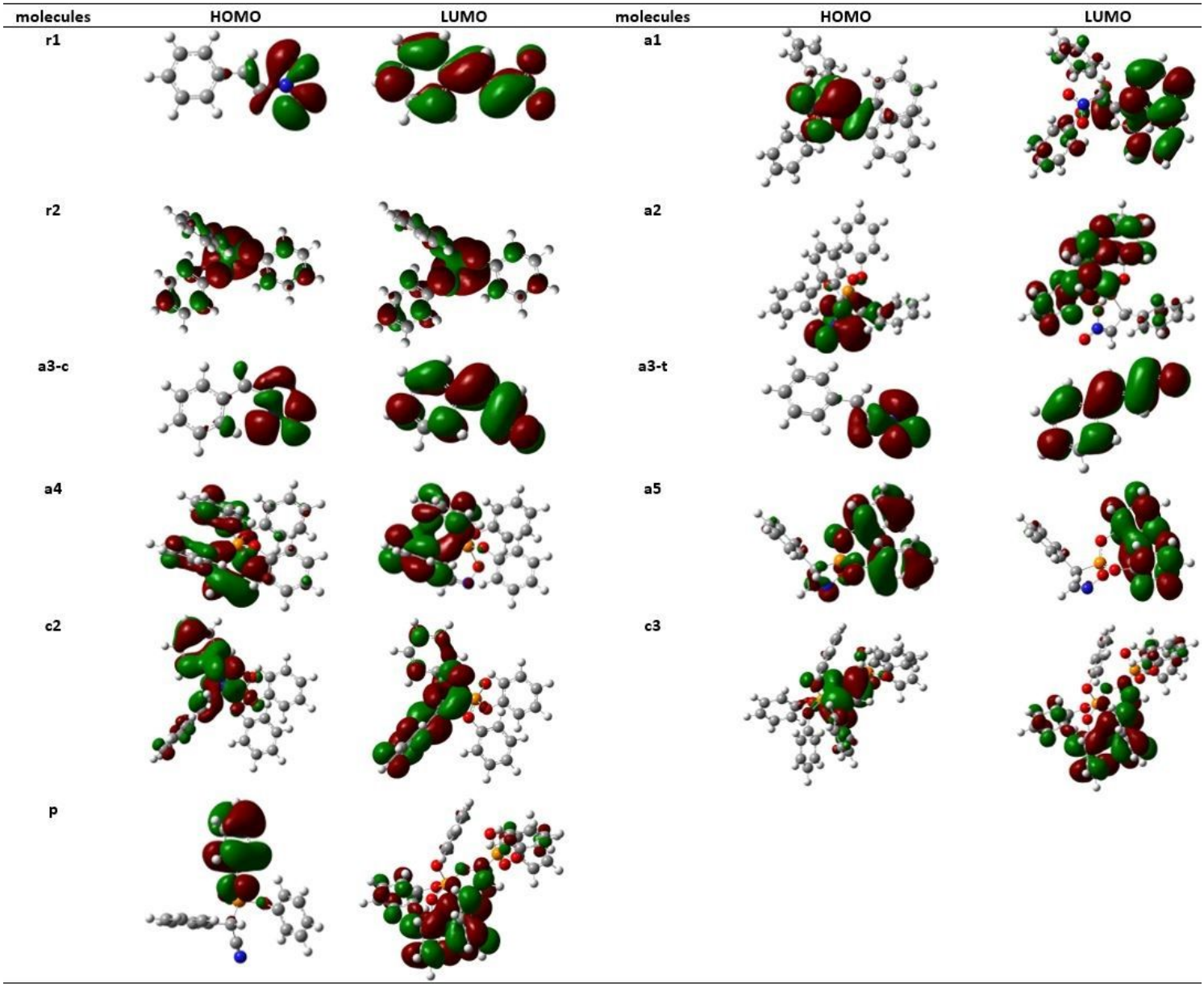

Figure 12

The structure of homo and lumo of compounds

Supplementary Files

This is a list of supplementary files associated with this preprint. Click to download.

- Scheme1.png
- Scheme2.png
- Scheme3.png
- Scheme4.png